MOLECULAR AND CELLULAR BIOLOGY, Sept. 2005, p. 8356–8367 Vol. 25, No. 18
0270-7306/05/$08.00+0 doi:10.1128/MCB.25.18.8356–8367.2005

The *RASSF1A* Isoform of *RASSF1* Promotes Microtubule Stability and Suppresses Tumorigenesis

L. van der Weyden,[1] K. K. Tachibana,[2]† M. A. Gonzalez,[2]† D. J. Adams,[1]†
B. L. Ng,[1] R. Petty,[1] A. R. Venkitaraman,[2] M. J. Arends,[3]
and A. Bradley[1]*

Mouse Genomics Lab, Wellcome Trust Sanger Institute, Wellcome Trust Genome Campus, Cambridge, United Kingdom[1]; MRC Cancer Cell Unit, Hutchinson/MRC Research Centre, Hills Road, Cambridge, United Kingdom[2]; and Department of Pathology, University of Cambridge, Addenbrooke's Hospital, Cambridge, United Kingdom[3]

Received 10 February 2005/Returned for modification 23 March 2005/Accepted 30 June 2005

The *RASSF1A* isoform of *RASSF1* is frequently inactivated by epigenetic alterations in human cancers, but it remains unclear if and how it acts as a tumor suppressor. RASSF1A overexpression reduces in vitro colony formation and the tumorigenicity of cancer cell lines in vivo. Conversely, RASSF1A knockdown causes multiple mitotic defects that may promote genomic instability. Here, we have used a genetic approach to address the function of RASSF1A as a tumor suppressor in vivo by targeted deletion of *Rassf1A* in the mouse. *Rassf1A* null mice were viable and fertile and displayed no pathological abnormalities. *Rassf1A* null embryonic fibroblasts displayed an increased sensitivity to microtubule depolymerizing agents. No overtly altered cell cycle parameters or aberrations in centrosome number were detected in *Rassf1A* null fibroblasts. *Rassf1A* null fibroblasts did not show increased sensitivity to microtubule poisons or DNA-damaging agents and showed no evidence of gross genomic instability, suggesting that cellular responses to genotoxins were unaffected. *Rassf1A* null mice showed an increased incidence of spontaneous tumorigenesis and decreased survival rate compared with wild-type mice. Irradiated *Rassf1A* null mice also showed increased tumor susceptibility, particularly to tumors associated with the gastrointestinal tract, compared with wild-type mice. Thus, our results demonstrate that *Rassf1A* acts as a tumor suppressor gene.

Loss of heterozygosity (LOH) at chromosome 3p21.3 is extremely common in human carcinomas of the lung and breast (14) and is believed to be a critical early event in the pathogenesis of lung cancer (11, 42). Comparative analysis of deletions in this region in lung and breast cancer cell lines has identified a critical deletion interval of 120 kb containing eight genes (14). While none of the genes in this deletion region are mutated at a significant frequency in cancer (14), one of these genes, *RASSF1*, is a strong candidate as the major tumor suppressor gene on the basis of its frequent epigenetic silencing and LOH in lung cancers (6).

The two major isoforms of RASSF1, A and C, are produced by alternative promoter usage and mRNA splicing (2, 6). Transcripts from both isoforms share four common exons (exons 3 to 6), which encode a Ras association (RA) domain, PEST sequences, and a consensus phosphorylation site for ataxia telangiectasia-mutated (ATM) kinase (6). Since the RASSF1 RA domain can associate with Ras oncoproteins in vitro (21) and ATM kinases play an essential role in DNA damage, RASSF1A/C may serve as a link between these two signaling pathways. Overexpression and knockdown studies of RASSF1 have implicated RASSF1A in regulating cell cycle progression and RASSF1C in Ras-mediated cellular activities. Both isoforms localize to the microtubules and the mitotic spindle, suggesting a possible involvement in regulating microtubule dynamics (39). Microtubules are protected against nocodazole-induced depolymerization by RASSF1A, and to some extent by RASSF1C, overexpression (39). The RASSF1 isoforms have been reported to play a role in mitotic progression; overexpression of RASSF1A but not RASSF1C causes a prometaphase arrest by preventing activation of the anaphase-promoting complex/cyclosome (APC/C), whereas short interfering RNA-mediated depletion of RASSF1A accelerates mitotic progression and causes mitotic defects (33). Furthermore, overexpression of RASSF1A has been shown in numerous studies to result in reduction of in vitro colony formation and anchorage-independent growth and reduction of the tumorigenicity of cancer cell lines in vivo (2, 6, 9). In contrast, only one study has reported that overexpression of RASSF1C resulted in growth inhibition in vitro and in vivo, and then only in the prostate and renal cell carcinoma cell lines LNCaP and KRC/Y, respectively, not the lung cancer line U2020 (15). These results suggest that RASSF1A function is distinct from RASSF1C and that *RASSF1A* may function as a tumor suppressor gene. Indeed, epigenetic inactivation of *RASSF1A* is frequently reported in human cancers (reviewed in reference 7) and in some cases has been shown to correlate with poor prognosis (17, 41, 43). In contrast, only one study has reported loss of expression of *RASSF1C* in cancer (38).

Here, we have generated *Rassf1A* null and conditional mice in order to dissect the functions attributed to the RASSF1 isoforms. We reexamine the role of RASSF1A in protecting microtubule stability and cell cycle progression and specifically examine the role of *RASSF1A* as a tumor suppressor gene.

* Corresponding author. Mailing address: Wellcome Trust Sanger Institute, Wellcome Trust Genome Campus, Hinxton, Cambridge CB10 1SA, United Kingdom. Phone: 44-(0)1223-834-244. Fax: 44-(0)1223-494-714. E-mail: abradley@sanger.ac.uk.
† These authors contributed equally.

MATERIALS AND METHODS

Construction of the *Rassf1A* targeting vector and generation of *Rassf1A* mutant mice. To generate the *Rassf1A* targeting vector (pAH19), DNA fragments for the 5′, conditional, and 3′ homology arms were amplified from AB2.2 genomic DNA by PCR using Platinum PCR Supermix High Fidelity (Invitrogen, San Diego, CA) for 10 to 18 cycles. The homology arms consisted of a 4.5-kb 5′ arm (containing the entire *BLU* gene [GenBank accession number AF333027] flanked by AscI sites), a 1.7-kb conditional arm (containing exon 1α flanked by HindIII sites), and a 4.4-kb 3′ homology arm (containing exons 1βγ, 2αβ, and 2γ flanked by NotI sites), which were cloned into pGEM T-Easy (Promega, Madison, WI), sequenced, and then subcloned into the AscI, HindIII, and NotI sites of pFlexible (36), respectively. Ten micrograms of the PvuI-linearized pAH19 was electroporated into 10^7 AB2.2 embryonic stem (ES) cells (from mouse strain 129S5/SvEvBrd) (24) and grown under 3-μg/ml puromycin selection. Cells were cultured on a lethally irradiated SNL76/7 feeder layer (18). ES clones were picked into 96-well plates after 9 days of drug selection and expanded, and targeted clones were identified by Southern blot analysis using PCR-amplified probes on NdeI- or SacII-digested genomic DNA with a 5′ or 3′ external probe, respectively. pAS3 is the 254-bp 5′ external probe (forward primer, 5′-TCT GGA GGG TGA GAC TCG GTT TTG TAA A-3′; reverse primer, 5′-TAC ATA GTG AGA CTT TGT CTC AGA AAA ATC AAC CTC CTT C-3′), and pAT1 is the 579-bp 3′ external probe (forward primer, 5′-GCT GAG ACT GAG CAG AAA ATC AAG GAC TAC AAT GG-3′, and reverse primer, 5′-CTT GGC CAT GCC GTT CAG TTC GCT CAA AGA GTG C-3′). The correctly targeted allele was termed *Rassf1A*^{Brdm1} (*m1*). To generate null and conditional alleles, a cell line with the *m1* allele was electroporated with 10 μg of a Cre-expressing plasmid (pTURBO-Cre; GenBank accession number AF334827) or an Flpe-expressing plasmid (pFLPe) (27), respectively. After 3 days of culture, the cells were trypsinized, reseeded at 3×10^5 cells/10-cm-diameter plate, and cultured in 0.2 μM 2-deoxy-2-fluoro-β-D-arabinofuranosyl-5-iodouracil (FIAU) for 5 days. After this time, the cells were grown for a further 3 days in drug-free medium before the resulting colonies were trypsinized, pooled, and analyzed by Southern blotting using the pAS3 probe on KpnI-digested genomic DNA or using the pR20P probe (a 1.2-kb PstI fragment from the conditional arm) on HindIII-digested genomic DNA. The allele in the Flp-transfected clones showing loss of the 12.1-kb KpnI fragment but not the 1.7-kb HindIII fragment was termed *Rassf1A*^{Brdc1} (*c1*) ("conditional" allele). The allele generated with Cre, which showed a 9.1-kb KpnI fragment and loss of the 1.7-kb HindIII fragment, was termed *Rassf1A*^{Brdm2} (*m2*) ("null" allele). ES cell clones for the null and conditional alleles were transmitted through the germ line and bred to homozygosity (maintained on a mixed 129/Sv-C57BL/6 background). Mice were housed in accordance with Home Office regulations (United Kingdom). For tumor induction studies mice were whole body irradiated with a sublethal dose of 3.5 Gy at 4 weeks of age.

Genotyping of *Rassf1A* mutant mice by genomic PCR. Genomic DNA was amplified in 50-μl reaction mixtures using 45 μl Platinum PCR Supermix (Invitrogen) and 100 ng of each primer pair (RSF-5/RSF-3 or RSF-C/RSF-3). The primers were as follows: RSF-3 (reverse primer), 5′-CCA GGC TTC CTT CTC ACT CCT CTG CCG C-3′; RSF-5 (forward primer), 5′-CTC GCC CCT GTC AGA CCT CAA TTT CCC-3′; and RSF-C (forward primer), 5′-AAG GAG AAA GAA AGC TGC TCT GGG GTT CT-3′. The PCR cycle profile was as follows: 1 cycle at 94°C for 2 min followed by 30 cycles at 94°C for 30 s, 65°C for 1 min, and 72°C for 30 s, with a final cycle of 72°C for 10 min.

Reverse transcriptase PCR (RT-PCR). RNA was extracted from +/+, *c1*/*c1*, and *m2*/*m2* mouse lung (RNAqueous; Ambion, Austin, TX), and 1.5 μg of total RNA was used to generate cDNA (RETROscript; Ambion). Specific primers were as follows: for *Rassf1A* exons 1α, 1βγ, and 2αβ (330-bp product), 5′-ATG TCG GCG GAG CCA GAA CTC ATT GAA CTA-3′ and 5′-CAC GTT CGT ATC CCG CTC TAG TGC AGA GT-3′; for *Rassf1C* exons 2γ and 3 (220-bp product), 5′-ATG GGC GAG GCT GAA ACA CCT TCC TTC GAA-3′ and 5′-CAG GCT CAT GAA GAG GTT GCT GTT GAT CT-3′; for *Rassf1* exons 3 and 4 (372-bp product), 5′-GAT GAG GCT GTA GAG CGG GAG ACA CCC G-3′ and 5′-CTT GGC CAT GCC GTT CAG TTC GCT CAA AG-3′; and for β-*actin* exons 2 and 3 (215-bp product), 5′-ACC AAC TGG GAC GAT ATG GAG AAG A-3′ and 5′-TAC GAC CAG AGG CAT ACA GGG ACA A-3′. The cDNA was amplified in 50-μl reaction mixtures using 45 μl Platinum PCR Supermix (Invitrogen) and 100 ng of each primer pair with the following PCR cycle profile: 1 cycle at 94°C for 2 min followed by 30 cycles at 94°C for 30 s, 65°C for 1 min, and 72°C for 30 s, with a final cycle of 72°C for 10 min. All PCR products were cloned into pGEM T-Easy and sequenced to confirm their identity.

Quantitative RT-PCR. RNA was extracted from +/+ and *m2*/*m2* mouse liver (Trizol; Invitrogen), and 5 μg of total RNA was used to generate cDNA (Superscript II reverse transcriptase; Invitrogen). Quantitative PCR (qPCR) was carried out using the relative quantitation comparative C_T method in separate tubes on the ABI 7900HT sequence detection system in accordance with the manufacturer's instructions (ABI user bulletin no. 2; Applied Biosystems, Foster City, CA). The target sequence was designed to exons 1 and 2 of *Rassf1C* (5′-AGC ACA ACC AGC AGT GGC TA-3′ and 5′-TTG ATT TTC TGC TCA GTC TCA-3′; 167-bp product), and the reference PCR product was designed to exons 3 and 4 of β-*actin* (5′-GAT CTG GCA CCA CAC CTT CT-3′ and 5′-GGG GTG TTG AAG GTC TCA AA-3′; 138-bp product). Both PCR products were tested to confirm the presence of a single clean product by gel electrophoresis and melt curve analysis on the ABI 7900HT sequence detection system. A validation experiment was carried out to confirm that the PCR efficiencies of the two products were sufficiently similar. qPCRs were performed with the QuantiTect Syber Green PCR kit (QIAGEN, Valencia, CA) in accordance with the manufacturer's instructions, using a 50-μl PCR volume, 5 ng cDNA, and 125 ng (2.5 ng/μl) primer. Five replicates of all PCRs were carried out, and the final quantification was determined relative to RNA from a wild-type mouse. The PCR products after qPCR were checked by melt curve analysis and gel electrophoresis to confirm the presence of a single clean product. The data are represented as the mean relative quantities of *Rassf1C* mRNA ± standard deviations (SD) (using liver RNA samples from four mice of each genotype).

Cell cycle and CD antigen analysis of thymocytes. Thymuses and spleens were excised from 6- to 7-week-old wild-type and *Rassf1A* null (*m2*/*m2*) mice and were gently crushed through 100-μm cell strainers (BD Falcon, Bedford, MA) in phosphate-buffered saline (PBS). After centrifugation and washing with PBS/2% fetal bovine serum, cells were divided into two groups for analysis. For analysis of CD antigen expression, cells were stained with CD2-fluorescein isothiocyanate (FITC), CD4-phycoerythrin (PE), CD8-FITC, and/or CD45R (B220)-FITC (Pharmingen, Palo Alto, CA) and analyzed by flow cytometry (20,000 cells examined per sample). For cell cycle analysis, cells (1.5×10^6) were fixed with 70% ethanol for 30 min at 4°C, RNase A treated (2 μg/ml; Sigma, St. Louis, MO) for 30 min at room temperature, and stained with propidium iodide (50 μg/ml; Sigma), and the DNA content was analyzed by flow cytometry. All fluorescence-activated cell sorter (FACS) data analysis was performed using WinMDI version 2.8 software.

Micronucleus assay. Blood was collected from wild-type and *Rassf1A* null 6- to 7-week-old and 7-month-old mice by cardiac puncture during terminal anesthesia and immediately fixed in methanol overnight at −80°C. DNA, CD71 antibody staining, and FACS analysis were performed using MicroFlow reagents from Litron Laboratories (Rochester, NY) as described by the manufacturer. Fifty thousand red cells were examined from each animal. For irradiation studies, 6- to 7-week-old mice were whole body irradiated at 0.7 Gy and blood was collected 48 h later.

Histology. Tissues from wild-type and *Rassf1A* null mice were collected and fixed in 10% neutral buffered formalin. Tissue samples were processed routinely and embedded in paraffin, sectioned at 4 μm, stained with hematoxylin and eosin, and analyzed by light microscopy.

Cell growth and proliferation of MEFs. Mouse embryonic fibroblasts (MEFs) were derived from 13.5-day-old embryos as described previously (29). All studies were performed on four to seven independently collected batches of MEFs, which were cultured up to passage 7 (P7). For cell growth assays MEFs were seeded in triplicate at a density of 3×10^5 cells/6-cm-diameter plate at day 0. Cells were counted daily using a Coulter counter (Beckman Coulter, Fullerton, CA). Data were collected from cell counts of four independent experiments.

Survival assays. Cytotoxicity was evaluated using the MTT (3-[4,5-dimethylthiazol-2-yl]-2,5 diphenyl tetrazolium bromide) assay, in which 4×10^3 wild-type or *Rassf1A* null MEFs in 200 μl of complete medium were placed into each well of a 96-well plate and 24 h later were exposed to a DNA-damaging agent (methyl methanosulfonate [MMS], mitomycin C [MMC], hydroxyurea [HU], ionizing radiation, or UV) or microtubule-binding agent (nocodazole, vinblastine, colchicine, or taxol). Exceptions include MMS treatment, in which cells were exposed to the drug for only 1 h, and ionizing radiation, in which cells were irradiated prior to plating. After 5 days, viability was assessed using CellTiter reagent (Promega), according to the manufacturer's recommendations. A minimum of eight wells were analyzed and averaged for each data point at each dose from four independent experiments. Results are expressed as means ± SD. All DNA-damaging and microtubule-binding chemicals were purchased from Sigma.

Spectral karyotyping. Spectral karyotyping analysis was carried out as previously described (31) on metaphase spreads prepared from wild-type and *Rassf1A* null MEFs (at P1) using the mouse SkyPaint probe mixture supplied by Applied Spectral Imaging (Vista, CA). Spectral images were captured using a Nikon

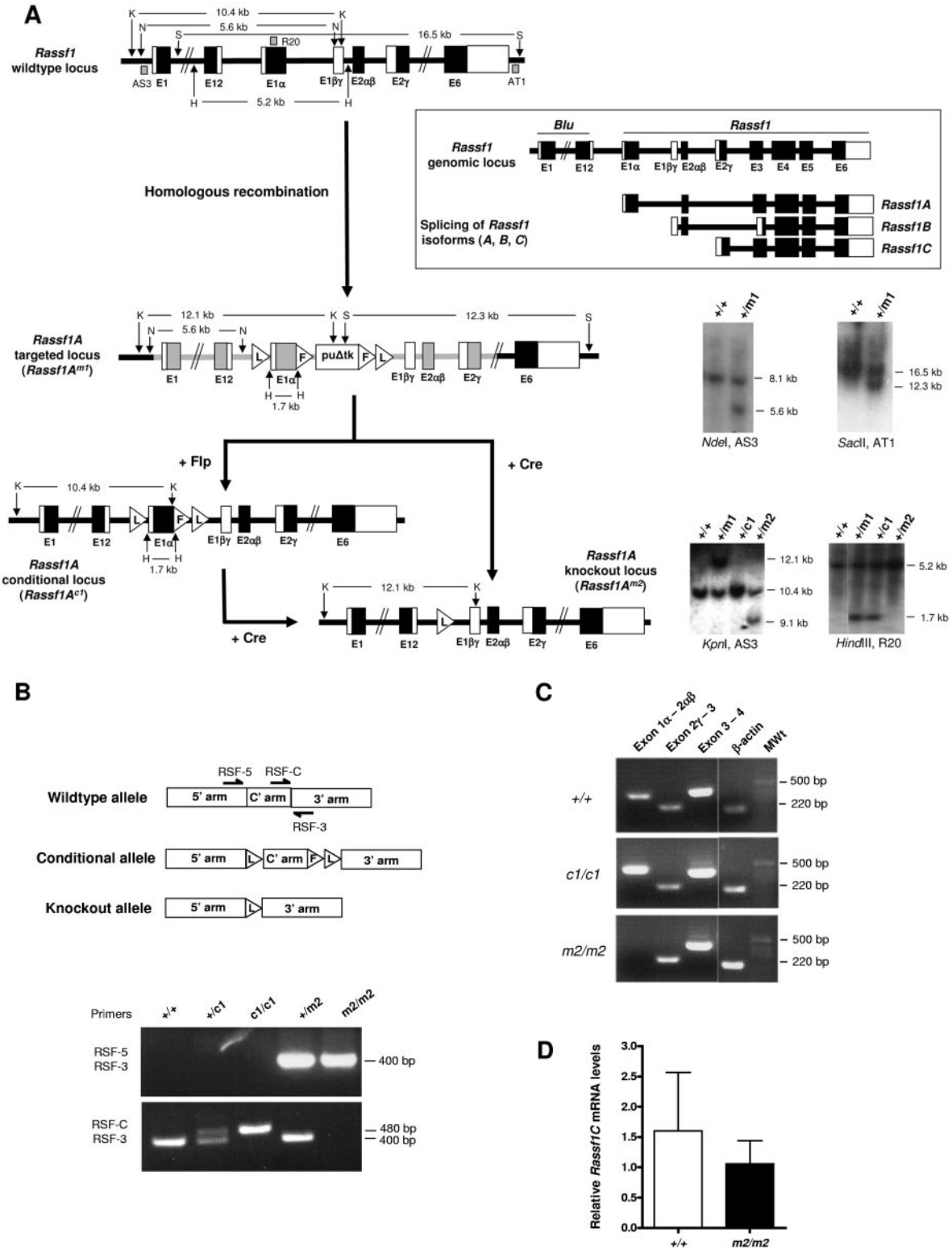

FIG. 1. Generation of null and conditional alleles of *Rassf1A*. A. (Box) Through the use of alternative promoter selection and alternative mRNA splicing of the *RASSF1* transcript, three isoforms have been described, namely, RASSF1A, RASSF1B, and RASSF1C (*RASSF1A* mRNAs also come in multiple tissue-related splice forms, including heart-specific RASSF1D [AF102771] and pancreas-specific RASSF1E [AF102772]) (2). However, the two major isoforms are the ubiquitously expressed RASSF1A and RASSF1C, as RASSF1B is hematopoietic cell specific. *RASSF1A* is a six-exon gene that initiates transcription at exon 1α. Thus to specifically ablate the *Rassf1A* isoform, *Lox*P (L) sites were positioned to allow Cre-mediated excision of exon 1α and generate a null knockout (*m2*) allele. The *puroΔtk* cassette, flanked by *FRT* (F) sites, can be excised using Flpe to generate a conditional (*c1*) allele. The regions of homology used in the targeting vector (pAH19) are shown in gray. *Blu* is a gene which

Eclipse E800 epifluorescence microscope equipped with an SD200 SpectraCube system (Applied Spectral Imaging). At least 20 raw spectral image files were acquired for each genotype using Spectral Imaging version 2.3 software (Applied Spectral Imaging) and analyzed using SkyView version 1.6.1 software (Applied Spectral Imaging).

Microtubule stability analysis. To evaluate microtubule stability in MEFs, cells were seeded onto polylysine-coated coverslips (Becton Dickinson) 24 h prior to treatment with nocodazole or colcemid for 30 min at 37°C. Coverslips were washed twice with cold PBS and were stained with mouse monoclonal anti-α-tubulin antibody at 1:200 (Molecular Probes, Eugene, OR) for 1 h at room temperature. After washing with PBS, Alexa Fluor 568-conjugated anti-mouse secondary antibody (Molecular Probes, Eugene, OR) was used and DNA was counterstained with Hoechst (Sigma). At each drug concentration, 100 to 150 cells were scored for microtubule integrity. Untreated cells have an extensive network of microtubule fibers that fills the cytoplasm. Local absence of defined fibers was scored as partial microtubule depolymerization, and the absence of any fibers was indicative of complete microtubule depolymerization. The micrographs shown are representative of >75% of the cells in terms of microtubule integrity at each concentration. Images were obtained with a Zeiss confocal microscope and processed using Photoshop 7.0 (Adobe Systems, San Jose, CA).

Immunofluorescence. MEFs were grown on polylysine-coated coverslips and pulsed with 40 μM bromodeoxyuridine (BrdU) for 1 h prior to fixation in 4% paraformaldehyde. Cells were permeabilized in 80% ethanol at −20°C and briefly in 0.1% Triton X-100/0.02% sodium dodecyl sulfate in PBS. Cells were blocked in 1% bovine serum albumin and stained with anti-BrdU and nuclease (Amersham Biosciences, Piscataway, NJ), rabbit anti-PH3 at 1:400 (Upstate Biotechnology, Waltham, MA), or rabbit anti-γ-tubulin 1:1,000 (Sigma). After washing with detergent, cells were incubated with Alexa Fluor 568-conjugated anti-mouse secondary antibody or Alexa Fluor 568-conjugated anti-rabbit secondary antibody (Molecular Probes). Hoechst (Sigma) was used to visualize DNA. At least 300 cells were scored for each experiment, and experiments were carried out with three to seven different batches of MEFs. When scoring cells for centrosome numbers, binucleate cells were excluded from the analysis. It was not possible to accurately determine the number of centrosomes in P7 MEFs as >80% of the cells contained no centrosomes (had been dispersed or degraded).

Statistics. For most comparisons, the Student *t* test (unpaired) was used to generate a *P* value. For the Kaplan-Meier curves, the log rank test was used.

RESULTS

Generation of *Rassf1A* null and conditional mice. To assess the physiologic role of RASSF1A, we used gene targeting to generate mice lacking *Rassf1A*. In contrast to a previous study in which *Rassf1* and hence all the isoforms were deleted (16) we specifically ablated the *Rassf1A* isoform by targeted deletion of exon 1α (Fig. 1A). Furthermore, we used a conditional approach to target *Rassf1A*, whereby the targeted locus contained *loxP* sites flanking exon 1α and *FRT* sites flanking the selection cassette (Fig. 1A). The conditional targeting vector was introduced into ES cells and correctly targeted clones, *Rassf1A*$^{+/Brdm1}$ (+/*m1*), were identified by Southern blotting (Fig. 1A). +/*m1* ES cell clones were then exposed to either Flpe (to delete the selection cassette) or Cre (to delete both exon 1α and the selection cassette) to generate the ES cell lines with the *Rassf1A*$^{+/Brdc1}$ (+/*c1*) and *Rassf1A*$^{+/Brdm2}$ (+/*m2*) alleles, respectively (Fig. 1A). These ES cell clones were used to generate chimeric mice that transmitted the mutated allele through the germ line. All offspring were genotyped by PCR using the strategy shown in Fig. 1B, which can distinguish between the five possible genotypes (+/+, +/*c1*, *c1*/*c1*, +/*m2*, and *m2*/*m2*).

***Rassf1A* null and conditional mice are viable, healthy, and fertile.** Interbreeding of heterozygous (+/*c1* or +/*m2*) mice produced homozygote conditional (*c1*/*c1*) and null (*m2*/*m2*) offspring at the expected Mendelian ratios. These mice were indistinguishable from littermate controls in terms of growth, development, and reproductive abilities. No histological differences could be seen between wild-type +/+, *c1*/*c1*, and *m2*/*m2* mice in all tissues examined (heart, lung, spleen, brain, thymus, kidney, stomach, intestine, pancreas, and testis; data not shown). RT-PCR performed on *m2*/*m2* lung cDNA confirmed the absence of *Rassf1A* exon 1α, while the other major isoform, *Rassf1C*, remained unaffected (Fig. 1C), as confirmed by quantitative RT-PCR (Fig. 1D). RT-PCR on *c1*/*c1* lung cDNA showed that the conditional allele was spliced appropriately, the *lox*P site in the intron following exon 1α did not interfere with splicing from exon 1α to exon 2αβ, and, given that *m2*/*m2* mice showed no obvious abnormalities, the *c1* allele was not characterized further. However, conditional inactivation of *Rassf1A* using the *c1*/*c1* mice will make it possible to evaluate the role of Rassf1A in specific tissues.

Lymphocyte development is normal in *Rassf1A* null mice. Rassf1A has been hypothesized to function as a negative regulator of cell cycle progression and cell proliferation (32). Given that tight cell cycle control is important for lymphocyte proliferation, we investigated the lymphocytic composition of thymuses and spleens from *Rassf1A* null mice. Loss of *Rassf1A* did not grossly affect thymic or splenic weight at either 6 to 7 weeks of age or 7 months of age (data not shown). Analysis of thymuses from *Rassf1A* null mice showed a thymocyte population comprising mainly double-positive ($CD4^+$ $CD8^+$) T cells, nearly identical to that of wild-type mice (Fig. 2A). Furthermore, similar proportions of mature $CD4^+$ and $CD8^+$ T cells were present in the spleens of wild-type and *Rassf1A* null mice (Fig. 2B). FACS analysis also demonstrated that the percentage of cells in the thymus and spleen that expressed CD2 (T-cell lineage) or CD45R (B220) (B-cell lineage) antigens, respectively, were unchanged in *Rassf1A* null mice (Fig. 2A). Thus, loss of *Rassf1A* gene function does not affect the lymphocytic component of the immune system.

***Rassf1A* null MEFs have no gross cell cycle defects.** Numerous studies performed using overexpression and short interfering RNA-mediated knockdown of RASSF1A in vitro have

lies adjacent to *Rassf1*. Southern blot analysis of the *Rassf1A* alleles was performed using three probes: pAS3 and pAT1, which are 5′ and 3′ of the targeted allele, respectively, and pR20, which is on the conditional allele. Restriction enzyme sites and fragment sizes are as indicated. H, HindIII; K, KpnI; N, NdeI; S, SacII. B. PCR genotyping of tail genomic DNA, using a combination of two primer pairs (either RSF-5/RSF-3 or RSF-C/RSF-3), can distinguish between all five genotypes (+/+, +/*c1*, *c1*/*c1*, +/*m2*, and *m2*/*m2*) based on the presence and size of the product(s), which can be resolved on a 2% agarose gel. C. RT-PCR was performed to confirm deletion of the floxed exons in *Rassf1A* null mice. RT-PCR performed on RNA extracted from +/+ and *c1*/*c1* mice shows a 330-bp product corresponding to *Rassf1A* exons 1α, 1βγ, and 2αβ. In contrast, no such product is seen in RNA from *m2*/*m2* mice. RNA from +/+, *c1*/*c1*, and *m2*/*m2* mice all show 220- and 372-bp products corresponding to exons 2γ and 3 and 3 and 4 of *Rassf1C* and *Rassf1* (common to all isoforms), respectively. β-*actin* was used as a positive control for cDNA production. D. Quantitative RT-PCR was performed to confirm there was no difference in the level of mRNA expression of the *Rassf1C* isoform between wild-type and *Rassf1A* null mice. Data are presented as mean relative levels of *Rassf1C* mRNA ± SD ($n = 4$).

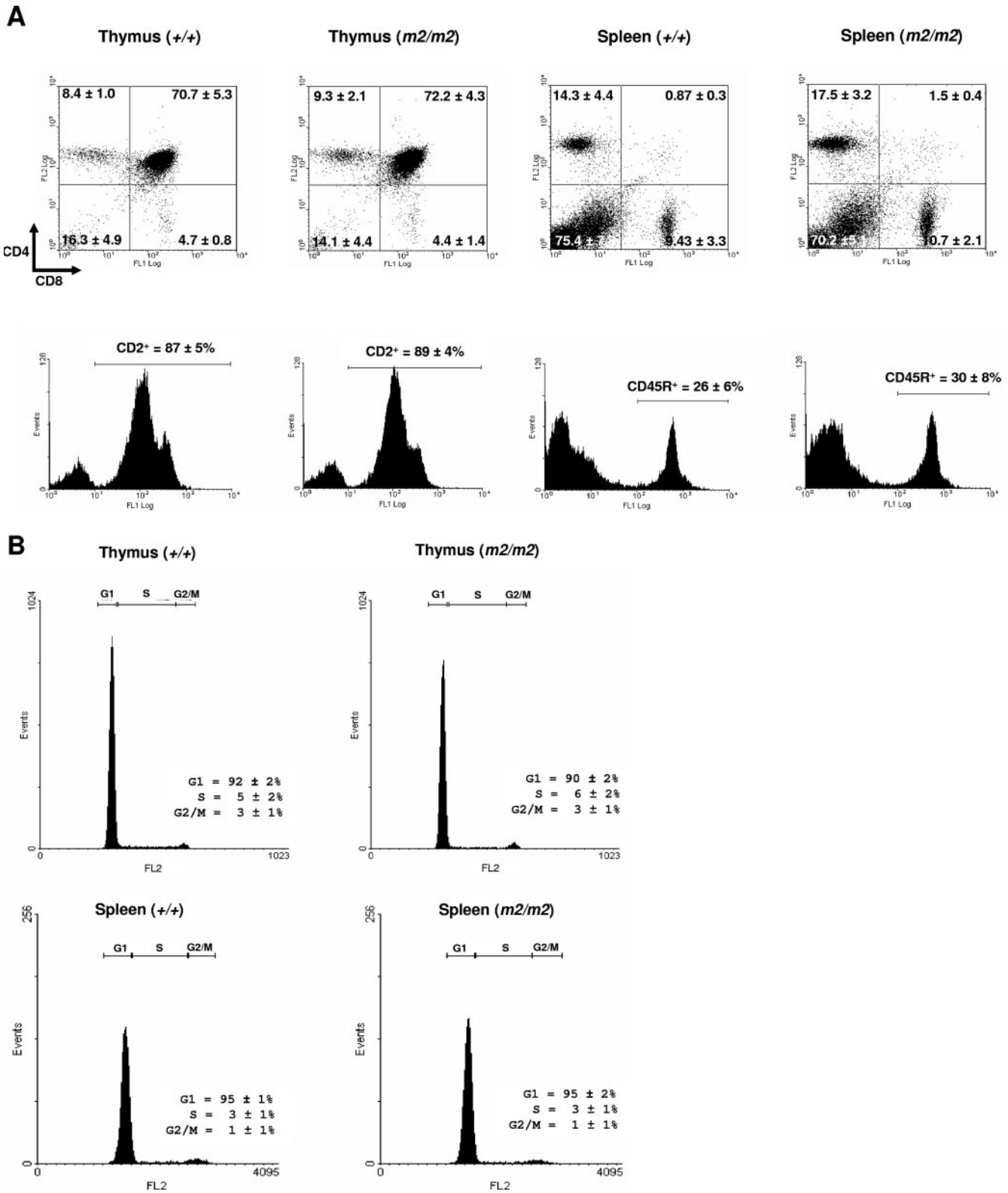

FIG. 2. Analysis of thymic and splenic lymphocytes in *Rassf1A* null and wild-type animals. A. Spleens and thymuses were taken from adult animals and stained with CD4-PI/CD8-FITC, CD2-FITC, or CD45R-FITC. A minimum of 10,000 events were analyzed from each organ. Data are presented as means ± SD ($n = 7$). B. Propidium iodide cell cycle analysis on thymic and splenic lymphocytes. A minimum of 10,000 events were analyzed from each organ. Data are presented as means ± SD ($n = 7$).

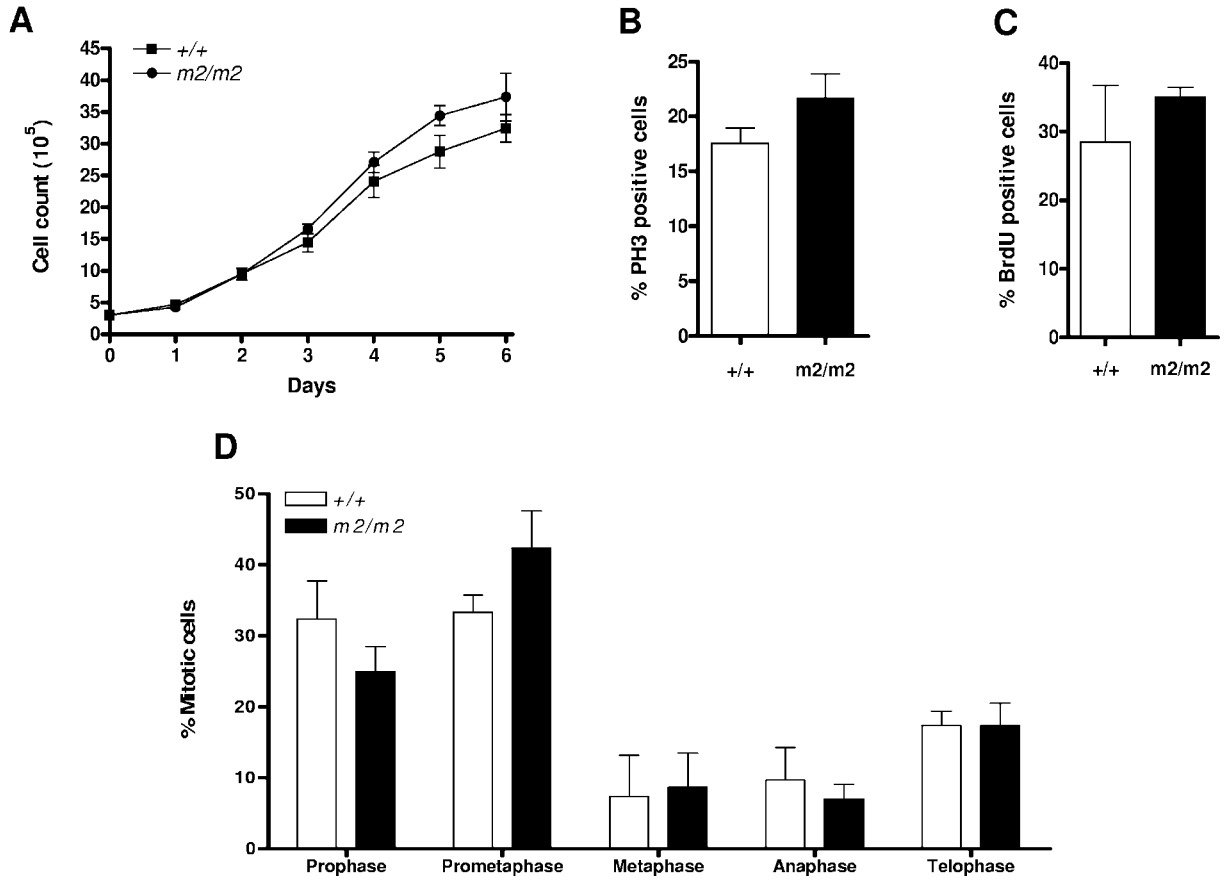

FIG. 3. Analysis of the cell cycle and mitotic properties of wild-type and *Rassf1A* null MEFs. A. Growth curves of wild-type (+/+) and *Rassf1A* null (*m2/m2*) MEFs. Cell counts were performed in triplicate at intervals of 24 h. Data represent means ± SD of four independently collected batches of MEFs. B. PH3 staining of wild-type and *Rassf1A* null MEFs to analyze the proportion of the population in G_2/M phase. At least 300 cells were scored for each experiment, and the data are presented as means ± SD ($n = 3$). C. BrdU staining of wild-type and *Rassf1A* null MEFs to analyze the proportion of the population in S phase. At least 300 cells were scored for each experiment, and the data are presented as means ± SD ($n = 3$). D. Analysis of the proportion of wild-type and *Rassf1A* null MEFs in each stage of mitosis. At least 200 cells were scored for each experiment, and the data are presented as means ± SD ($n = 3$).

implicated RASSF1A in playing a role in regulating cell cycle and mitotic progression (5, 25, 32, 33, 39). However, FACS analysis of propidium iodide-stained *Rassf1A* null and wild-type thymocytes, splenocytes, and MEFs did not show any accumulation of cells in a particular phase of the cell cycle (Fig. 2B and data not shown). There was also no difference in the growth curves of *Rassf1A* null and wild-type MEFs (Fig. 3A). Consistent with this, confocal microscopy of asynchronous *Rassf1A* null MEFs also showed no difference in the proportion of G_2/M phase cells identified by phosphorylated histone H3 (4) (Fig. 3B) or in S phase cells identified by BrdU incorporation (Fig. 3C). Transient knockdown of *Rassf1A* has been previously shown to decrease the time spent in mitosis, presumably by premature APC/C activation and faster progression toward anaphase (33). In *Rassf1A* null MEFs, cells in each mitotic phase were scored and no significant difference was found in the proportion of premetaphase to postmetaphase cells (Fig. 3D). A slight increase in prometaphase cells was detected in *Rassf1A* null MEFs, which may reflect difficulties in spindle assembly in the absence of Rassf1A. Thus the absence of Rassf1A does not result in overt misregulation of the cell cycle or mitotic progression.

***Rassf1A* null MEFs show an increased sensitivity to microtubule-depolymerizing agents.** Protection of microtubules by Rassf1 has been shown previously (5, 16, 39), and we demonstrate here that at least a portion of this activity can be attributed to the Rassf1A isoform. *Rassf1A* null MEFs showed more extensive depolymerization of the microtubule network at low concentrations of nocodazole compared to wild-type MEFs (32.2% ± 10.7% versus 10.5% ± 1.1% of cells depolymerized at 0.5 μM, respectively; Fig. 4). Microtubule fibers could still be detected at 1 μM nocodazole in wild-type cells but could hardly be seen in *Rassf1A* null MEFs at this concentration. Similar results were found with another microtubule-depolymerizing agent, colcemid (data not shown).

***Rassf1A* null mice show no evidence of genomic stability.** Transient knockdown of *Rassf1A* in foreskin fibroblasts has been shown to cause mitotic abnormalities including multiple centrosomes and lagging chromosomes that were postulated to contribute to genomic instability (33). However, *Rassf1A* null MEFs did not display lagging chromosomes (data not shown) or show distinct aberrations in centrosome numbers (P1 to P3), although at later passages (P5) a larger percentage of cells with more than two centrosomes was noticed than in wild-type cells

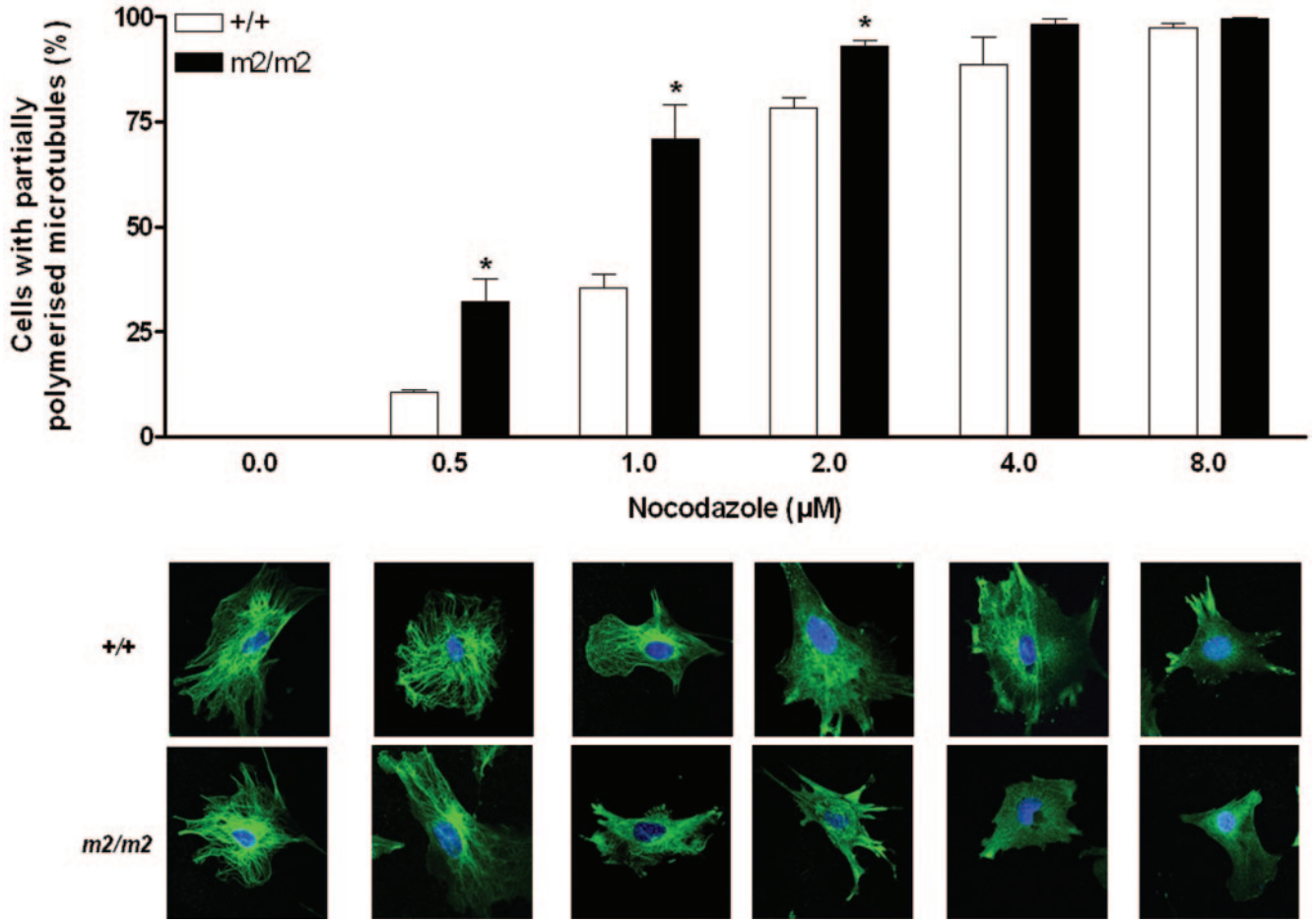

FIG. 4. *Rassf1A* null MEFs are more sensitive than wild-type MEFs to nocodazole-induced microtubule depolymerization. Wild-type and *Rassf1A* null (*m2*/*m2*) MEFs were incubated with nocodazole at the indicated concentrations for 30 min before staining with anti-α-tubulin antibody. At total of 100 to 150 cells were scored for each experiment, and the data are presented as means ± standard errors of the means ($n = 4$), with representative images shown for each concentration. Asterisk, $P < 0.05$ for +/+ versus *m2*/*m2* at the concentration indicated.

(though not significant by Student's *t* test analysis; Fig. 5A). A complete analysis of the total chromosome content using spectral karyotyping (SKY) of metaphase spreads from wild-type and *Rassf1A* null MEFs showed no evidence of gross chromosomal rearrangements or aneuploidy (Fig. 5B). To confirm the absence of aneuploidy in *Rassf1A* null MEFs, we used the highly sensitive flow-cytometric micronucleus assay, which provides a quantitative measure of in vivo chromosome damage (10). Micronuclei can arise from acentric chromosome fragments or whole chromosomes that have not been incorporated in the main nuclei at cell division (20). As shown in Fig. 5C, *Rassf1A* null mice at either 6 to 7 weeks (0.24% ± 0.08%, $n = 7$) or 7 months of age (0.30% ± 0.08%, $n = 4$) did not show higher levels of micronuclei than wild-type littermates (0.27% ± 0.06%, $n = 7$ and 0.31% ± 0.06%, $n = 6$, respectively). Since irradiation can stimulate micronucleus formation (1, 30), *Rassf1A* null mice at 6 to 7 weeks of age were irradiated with 0.7 Gy and blood was collected 48 h later. Still, irradiated *Rassf1A* null mice (2.5% ± 0.8%, $n = 7$) did not show significantly higher levels of micronuclei than irradiated wild-type littermates (2.0% ± 0.9%, $n = 7$; Fig. 5C). Taken together, these data suggest that the absence of Rassf1A does not result in gross genomic instability.

***Rassf1A* deficiency does not affect sensitivity to DNA-damaging or microtubule-binding agents.** To examine the effect of Rassf1A deficiency on cell growth and viability after DNA damage, we performed an MTT assay on *Rassf1A* null MEFs exposed to a variety of DNA-damaging agents, including irradiation to induce DNA double-strand breaks, UV to induce nucleotide alterations, and HU to inhibit DNA synthesis, as well as the DNA cross-linking agent MMC and the alkylating agent MMS. As shown in Fig. 6, *Rassf1A* null MEFs did not show increased sensitivity compared to wild-type MEFs to the induced forms of DNA damage or microtubule poisons. This phenotype was confirmed in another cell type, by performing clonogenic assays on double-targeted (*m2*/*m2*) ES cells (data not shown). Thus *Rassf1A* deficiency does not impair checkpoint responses triggered by DNA damage or failure to correctly assemble mitotic spindles.

***Rassf1A* deficiency plays a role in tumorigenesis.** Using our *Rassf1*A null mice, we addressed the key question of whether loss of Rassf1A is relevant in tumorigenesis. As shown in Fig.

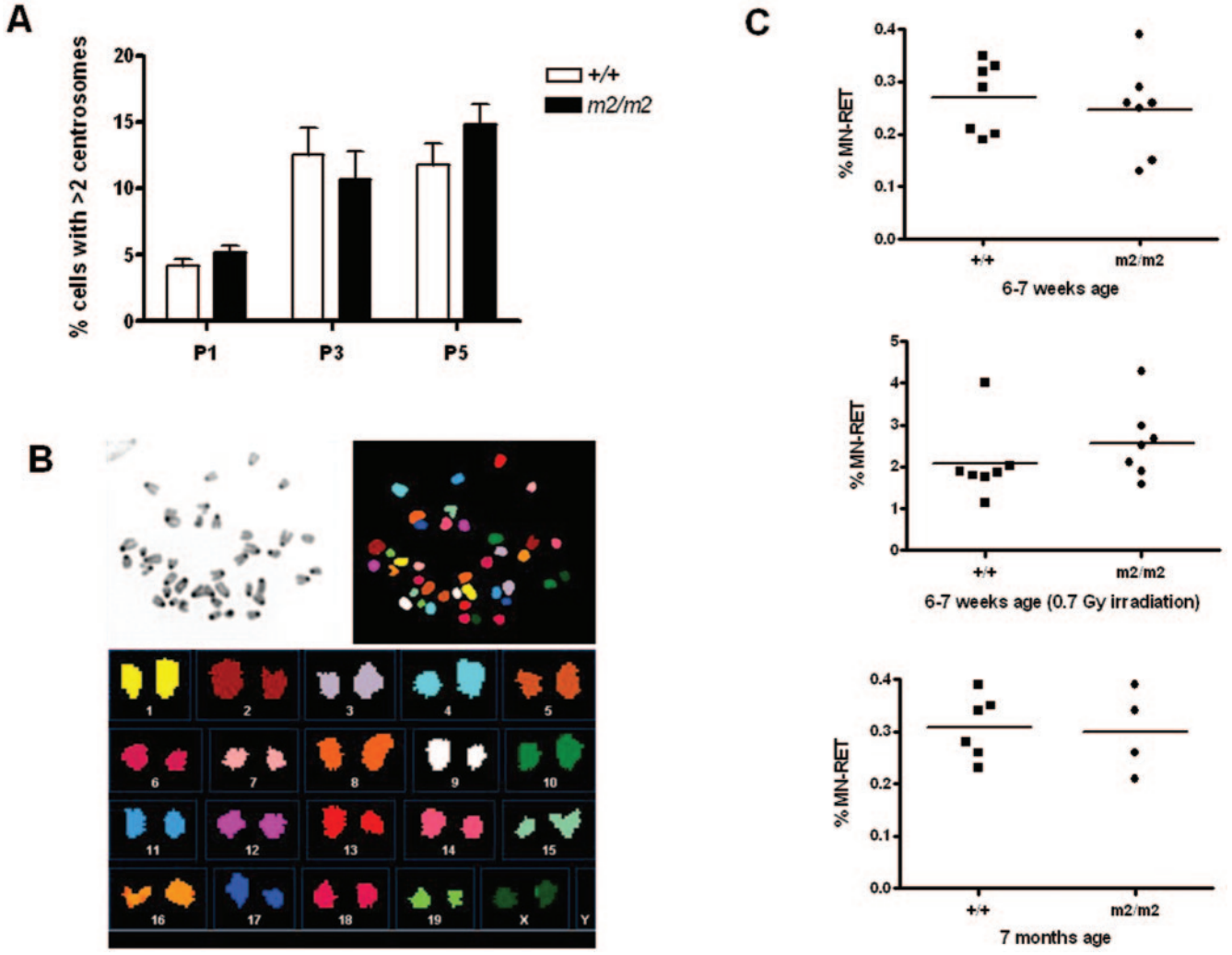

FIG. 5. *Rassf1A* null MEFS do not show evidence of increased genomic instability. A. Quantitation of centrosome numbers determined by γ-tubulin staining of wild-type and *Rassf1A* null (*m2*/*m2*) MEFs at P1, P3, and P5. At least 300 cells were scored for each experiment, and the data are presented as means ± SD ($n = 7$). B. SKY analysis. A SKY hybridization and detection kit was used to visualize the 19 autosomal and 2 sex chromosomes in colors. At least 20 raw spectral image files were acquired for each genotype, and images were analyzed using SkyView software. C. Micronucleus assays on blood from *Rassf1A* null and wild-type mice at 6 to 7 weeks of age (top), 6 to 7 weeks of age 48 h after irradiation with 0.7 Gy (center), and 7 months of age (bottom). Peripheral blood was stained with anti-CD71-FITC antibody and propidium iodide and analyzed by flow cytometry. A minimum of 50,000 events were analyzed for each sample. Data represent analysis of blood from four to seven animals of each genotype.

7A, *Rassf1A* null mice showed a significantly reduced rate of survival compared to wild-type littermates. In comparison to the death of 30% of the wild-type mice, 50% of the *Rassf1A* null mice died during the course of the study. In both cohorts the predominant cause of death was cancer, in particular lymphoma (Table 1). In addition to the deaths shown in Table 1, two *Rassf1A* null mice showed no tumors at the time of death (both died from cardiac failure and pneumonia). To accelerate tumorigenesis, *Rassf1A* null mice were irradiated with 3.5 Gy at 4 weeks of age (Fig. 7B). Irradiated *Rassf1A* null mice showed an increased incidence of tumorigenesis and decreased survival rate compared with wild-type mice, with 27 of the 39 *Rassf1A* null mice dying (69%) compared to 24 of the 46 wild-type mice (52%). It is noteworthy that, although the majority of all tumors that developed were lymphomas, often with metastatic spread to many organs, *Rassf1A* null mice showed more tumor formation (adenomas and adenocarcinoma) in the gastrointestinal (GI) tract than wild-type mice (Fig. 7C).

DISCUSSION

RASSF1A methylation has been reported in almost all types of human cancer (reviewed in references 7 and 22). However, how *RASSF1A* functions as a tumor suppressor gene remains largely unknown. Recent work has suggested that RASSF1A might provide the crucial link between tumor suppression and the cell cycle (16, 33) by controlling the stability of microtubules and the activity of APC/C. To delineate the role of RASSF1A in the cell cycle and tumorigenesis, we have used a genetic approach and generated *Rassf1A* knockout mice. Due

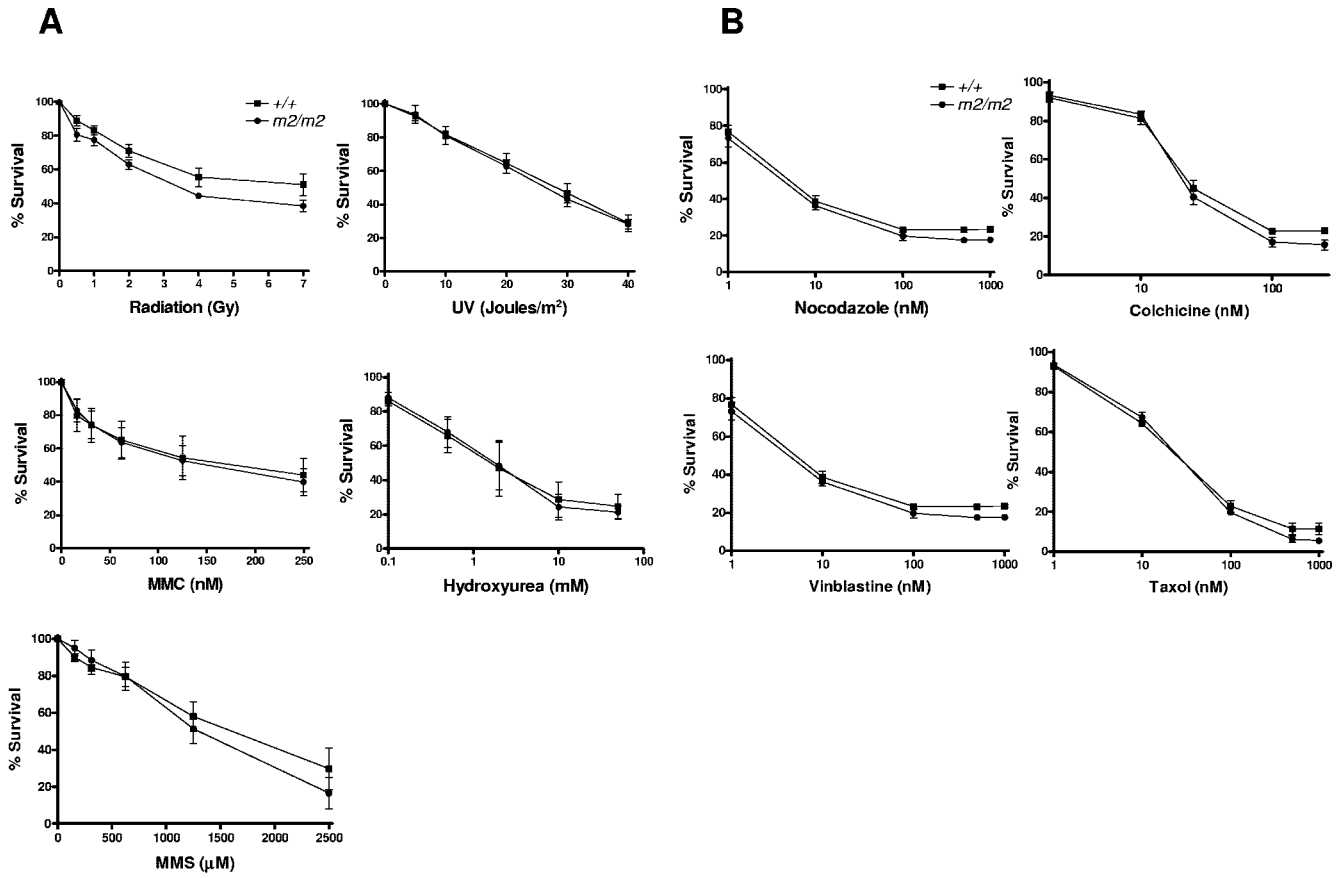

FIG. 6. *Rassf1A* null MEFs cells do not show an enhanced cytotoxicity to DNA damaging- and microtubule-binding agents. The cytoxicity of DNA-damaging and microtubule-binding agents on *Rassf1A* null MEFs was examined using the MTT assay in a 96-well format (as described in Materials and Methods). Treatments include the DNA-damaging agents irradiation, UV, MMS, MMC, and HU (A) and the microtubule-binding agents nocodazole, colchicine, vinblastine, and taxol (B). Data were normalized to untreated cells of the same genotype, and results are expressed as % survival (representing the means of four to six independent experiments ± standard errors of the means).

to concerns that the homozygous null mice may be embryonically lethal, we also generated a conditional *Rassf1A* allele. However, *Rassf1A* null mice unexpectedly proved to be viable, fertile, and healthy. Most surprisingly, loss of Rassf1A did not grossly impair cell cycle progression in vivo. Lymphocytes from *Rassf1A* null mice were identical to those from wild-type littermates in terms of proportions of T and B lymphocytes and showed no difference in the proportion of cells in each cell cycle phase. The growth kinetics and cell cycle profiles of *Rassf1A* null MEFs were indistinguishable from wild-type MEFs. A closer, but stationary, analysis of the mitotic phases revealed a subtle difference between *Rassf1A* null and wild-type MEFs in the prometaphase population, the stage during which spindle assembly occurs. Protection of microtubules by *Rassf1* has been shown previously (5, 39), and we demonstrate that at least a portion of this activity can be attributed to the *Rassf1A* isoform. This is consistent with the recent finding that RASSF1C can bind tubulin but is far less effective than RASSF1A at stabilizing microtubules (39).

The viability of the *Rassf1A* null mouse and the absence of any obvious cell cycle defects are perhaps not altogether that surprising, as the traditional view of the mammalian cell cycle depicts many components as fulfilling essential steps that dictate the sequential order of cell cycle events, yet *Cyclin E*, *Cyclin D*, *Cdk2*, *Cdk4*, and *Cdc25C* knockout mice have all been shown to be viable (reviewed in reference 34). Reasons for this could include compensation by other proteins with similar activity or the fact that some of these gene products have major roles but only in specific cell lineages. Other reasons could lie in the fact that most of the studies that declare genes to be essential for regulation of the cell cycle stem from analysis of cultured cells, many of which have defects in other key regulatory genes. This is particularly relevant for RASSF1A, as studies on the role of RASSF1A in the cell cycle have largely been performed using transformed immortalized cells such as HeLa cells, which have an abrogated Rb checkpoint due to human papillomavirus E7 expression, or H1299 cells, which are p53 null. Therefore, these cells lack many of the normal growth control regulations that would be imposed on a cell in vivo.

Previous in vitro observations using *RASSF1A* mutant cDNAs or transient knockdown of *RASSF1A* have led to the hypothesis that an absence of RASSF1A results in genomic instability (16, 33, 39). However, *Rassf1A* null mice did not display increased genomic instability or abrogation of DNA repair pathways. This lack of susceptibility to aneuploidy is

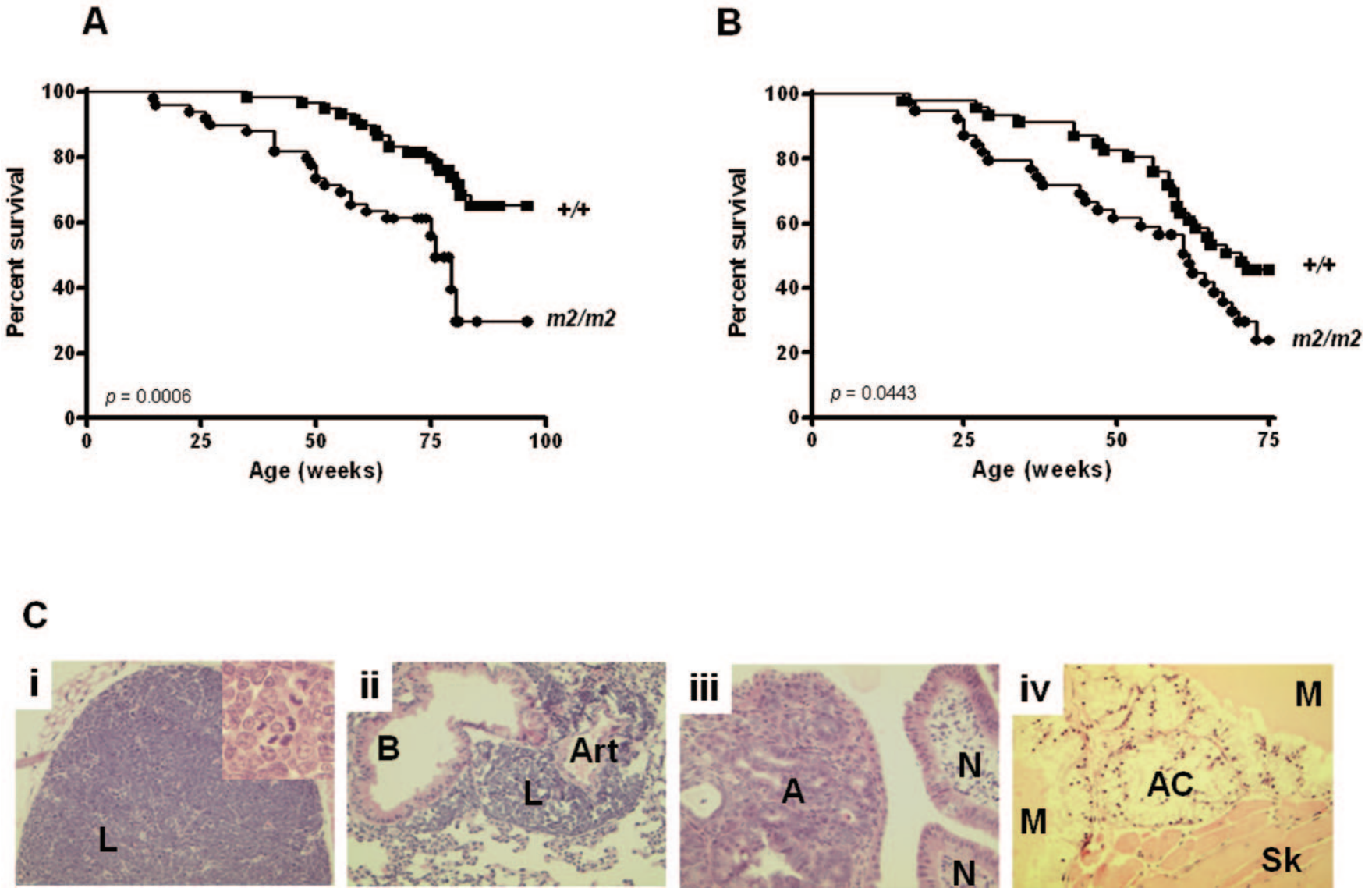

FIG. 7. *Rassf1A* null mice develop tumors with and without irradiation. Kaplan-Meier plots show the percentages of survival of wild-type (+/+) and *Rassf1A* null (*m2*/*m2*) mice in the (A) nonirradiated and (B) irradiated cohorts. C. Hematoxylin- and eosin-stained sections (×180 magnification) showing tumor formation. (i) thymic lymphoma (L), high grade, confined to thymus (*m2*/*m2*, irradiated; inset: high-grade lymphoma cells with many mitotic figures shown at high-power view [×360]); (ii) metastatic lymphoma (L) in lung, with high-grade lymphoma surrounding a bronchus (B) and artery (Art) (*m2*/*m2*, irradiated); (iii) small intestinal adenoma (A) (left) with adjacent normal intestinal villi (N) (right) (*m2*/*m2*, irradiated); (iv) metastatic mucinous adenocarcinoma (AC) producing pale-yellow-staining mucin (M) and invading skeletal muscle (Sk) (bottom right) of groin (*m2*/*m2*, nonirradiated).

TABLE 1. Tumors found in wild-type and *Rassf1A* null mice[a]

Type and site of tumor	No. of mice			
	Spontaneous		Irradiated	
	+/+	*m2*/*m2*	+/+	*m2*/*m2*
Lymphoma/leukemia	14	17	18	20
Carcinoma				
Adenocarcinoma				
Ovary			1	
Lung	1	2	4	1
Gl tract		1		
Squamous carcinoma of skin			1	
Sarcoma				
Angiosarcoma	1	2	1	2
Osteogenic		1		1
Benign				
Adenoma				
Adrenal glands			1	
Lung			1	
Gl tract			1	2
Lipoma	1			
Myxoma			1	
Pheochromocytoma				1
Sex cord tumor (ovary)				1

[a] This table represents the different tumor types that were found; hence mice that developed multiple tumors are represented more than once. For the spontaneous cohort, 24 of the 48 *Rassf1A* null (*m2*/*m2*) mice died (50%) compared to 18 of the 59 wild-type mice (30%). For the irradiated cohort, 27 of the 39 *Rassf1A* null (*m2*/*m2*) mice died (69%) compared to 24 of the 46 wild-type mice (52%).

unlikely to be due to functional compensation by Rassf1C, as *Rassf1* null MEFs have also been reported to show no gross chromosomal aberrations (16). A more likely explanation is that, in order for a cell with such severe chromosomal abnormalities to be able to exist, defects in other key checkpoint (tumor suppressor) genes would also need to be present.

We addressed the key question of whether loss of *Rassf1A* is relevant in tumorigenesis. *Rassf1A* null mice showed a significantly increased incidence of tumorigenesis compared to wild-type littermates. Irradiated *Rassf1A* null mice also showed a reduced rate of survival and increased incidence of tumorigenesis, compared to irradiated wild-type mice. Irradiated heterozygous *Rassf1A* mice (+/*m2*) did not show an increased incidence of tumorigenesis or decreased rate of survival compared to wild-type mice; however, given the small size of this cohort (3 of the 12 mice [25%] developed tumors) the possibility of a haploinsufficiency effect cannot be excluded. In both the irradiated and nonirradiated cohorts, although the predominant tumor type was lymphoma, *Rassf1A* null mice showed additional tumors associated with the gastrointestinal tract, not commonly seen in the wild-type mice. Well-differentiated endocrine carcinomas of gastric origin have been shown to have frequent alterations in 3p21 (23), and epigenetic transcriptional silencing of *RASSF1A* is a frequent event in gastric tumorigenesis and might play an important role in the malignant progression of gastric adenocarcinomas (3, 12, 35). In addition, *RASSF1A* methylation has also been reported in colorectal cancer and hepatocellular carcinomas (13, 26, 28, 37, 40, 44). Interestingly, these are the same tumor types in which promoter methylation of the *APC* gene (adenomatous polyposis coli [APC]) has also been reported (13). Given that APC stimulates microtubule assembly and bundling (19, 45) and that lack of microtubule binding associated with cancer-associated mutations of *APC* are believed to contribute to defects in the assembly of mitotic spindles and lead to missegregation of chromosomes (8), it is tempting to speculate that aberrant APC function may play a role in the neoplastic progression of gastrointestional tract tissues with methylated or inactivated *RASSF1A*.

ACKNOWLEDGMENTS

L.V.D.W. and D.J.A. are recipients of Australian NHMRC postdoctoral research fellowships (CJ Martin/RG Menzies Fellowship and CJ Martin Fellowship, respectively). K.K.T. is supported by an MRC predoctoral fellowship, M.A.G. is supported by an MRC clinical research training fellowship, and M.J.A. is supported by Cancer Research UK. This research was supported by the Wellcome Trust.

We thank Ron Laskey for helpful discussions, Ian Roberts for assistance with cytogenetic analysis, Graham Bignell for assistance with quantitative RT-PCR experiments, Evelyn Grau for microinjection of the targeted ES cell lines, and the personnel of Team 83 for care and monitoring of the animals.

REFERENCES

1. **Bhilwade, H. N., R. C. Chaubey, and P. S. Chauhan.** 2004. Gamma ray induced bone marrow micronucleated erythrocytes in seven strains of mouse. Mutat. Res. **560:**19–26.
2. **Burbee, D. G., E. Forgacs, S. Zochbauer-Muller, L. Shivakumar, K. Fong, B. Gao, D. Randle, M. Kondo, A. Virmani, S. Bader, Y. Sekido, F. Latif, S. Milchgrub, S. Toyooka, A. F. Gazdar, M. I. Lerman, E. Zabarovsky, M. White, and J. D. Minna.** 2001. Epigenetic inactivation of RASSF1A in lung and breast cancers and malignant phenotype suppression. J. Natl. Cancer Inst. **93:**691–699.
3. **Byun, D. S., M. G. Lee, K. S. Chae, B. G. Ryu, and S. G. Chi.** 2001. Frequent epigenetic inactivation of RASSF1A by aberrant promoter hypermethylation in human gastric adenocarcinoma. Cancer Res. **61:**7034–7038.
4. **Crosio, C., G. M. Fimia, R. Loury, M. Kimura, Y. Okano, H. Zhou, S. Sen, C. D. Allis, and P. Sassone-Corsi.** 2002. Mitotic phosphorylation of histone H3: spatiotemporal regulation by mammalian Aurora kinases. Mol. Cell. Biol. **22:**874–885.
5. **Dallol, A., A. Agathanggelou, S. L. Fenton, J. Ahmed-Choudhury, L. Hesson, M. D. Vos, G. J. Clark, J. Downward, E. R. Maher, and F. Latif.** 2004. RASSF1A interacts with microtubule-associated proteins and modulates microtubule dynamics. Cancer Res. **64:**4112–4116.
6. **Dammann, R., C. Li, J. H. Yoon, P. L. Chin, S. Bates, and G. P. Pfeifer.** 2000. Epigenetic inactivation of a RAS association domain family protein from the lung tumour suppressor locus 3p21.3. Nat. Genet. **25:**315–319.
7. **Dammann, R., U. Schagdarsurengin, M. Stunnikova, M. Rastetter, C. Seidel, L. Liu, S. Tommasi, and G. P. Pfeifer.** 2003. Epigenetic inactivation of the Ras-association domain family 1 (RASSF1A) gene and its function in human carcinogenesis. Histol. Histopathol. **18:**665–677.
8. **Dikovskaya, D., I. P. Newton, and I. S. Nathke.** 2004. The adenomatous polyposis coli protein is required for the formation of robust spindles formed in CSF *Xenopus* extracts. Mol. Biol. Cell **15:**2978–2991.
9. **Dreijerink, K., E. Braga, I. Kuzmin, L. Geil, F. M. Duh, D. Angeloni, B. Zbar, M. I. Lerman, E. J. Stanbridge, J. D. Minna, A. Protopopov, J. Li, V. Kashuba, G. Klein, and E. R. Zabarovsky.** 2001. The candidate tumor suppressor gene, RASSF1A, from human chromosome 3p21.3 is involved in kidney tumorigenesis. Proc. Natl. Acad. Sci. USA **98:**7504–7509.
10. **Heddle, J. A.** 1973. A rapid in vivo test for chromosomal damage. Mutat. Res. **18:**187–190.
11. **Hung, J., Y. Kishimoto, K. Sugio, A. Virmani, D. D. McIntire, J. D. Minna, and A. F. Gazdar.** 1995. Allele-specific chromosome 3p deletions occur at an early stage in the pathogenesis of lung carcinoma. JAMA **273:**558–563.
12. **Kang, G. H., S. Lee, J. S. Kim, and H. Y. Jung.** 2003. Profile of aberrant CpG island methylation along multistep gastric carcinogenesis. Lab. Investig. **83:**519–526.
13. **Lee, S., H. J. Lee, J. H. Kim, H. S. Lee, J. J. Jang, and G. H. Kang.** 2003. Aberrant CpG island hypermethylation along multistep hepatocarcinogenesis. Am. J. Pathol. **163:**1371–1378.
14. **Lerman, M. I., and J. D. Minna.** 2000. The 630-kb lung cancer homozygous deletion region on human chromosome 3p21.3: identification and evaluation of the resident candidate tumor suppressor genes. The International Lung CancerChromosome 3p21.3 Tumor Suppressor Gene Consortium. Cancer Res. **60:**6116–6133.
15. **Li, J., F. Wang, A. Protopopov, A. Malyukova, V. Kashuba, J. D. Minna, M. I. Lerman, G. Klein, and E. Zabarovsky.** 2004. Inactivation of RASSF1C during in vivo tumor growth identifies it as a tumor suppressor gene. Oncogene **23:**5941–5949.

16. **Liu, L., S. Tommasi, D. H. Lee, R. Dammann, and G. P. Pfeifer.** 2003. Control of microtubule stability by the RASSF1A tumor suppressor. Oncogene **22:**8125–8136.
17. **Maruyama, R., S. Toyooka, K. O. Toyooka, K. Harada, A. K. Virmani, S. Zochbauer-Muller, A. J. Farinas, F. Vakar-Lopez, J. D. Minna, A. Sagalowsky, B. Czerniak, and A. F. Gazdar.** 2001. Aberrant promoter methylation profile of bladder cancer and its relationship to clinicopathological features. Cancer Res. **61:**8659–8663.
18. **McMahon, A. P., and A. Bradley.** 1990. The Wnt-1 (int-1) proto-oncogene is required for development of a large region of the mouse brain. Cell **62:**1073–1085.
19. **Munemitsu, S., B. Souza, O. Muller, I. Albert, B. Rubinfeld, and P. Polakis.** 1994. The APC gene product associates with microtubules in vivo and promotes their assembly in vitro. Cancer Res. **54:**3676–3681.
20. **Nusse, M., B. M. Miller, S. Viaggi, and J. Grawe.** 1996. Analysis of the DNA content distribution of micronuclei using flow sorting and fluorescent in situ hybridization with a centromeric DNA probe. Mutagenesis **11:**405–413.
21. **Ortiz-Vega, S., A. Khokhlatchev, M. Nedwidek, X. F. Zhang, R. Dammann, G. P. Pfeifer, and J. Avruch.** 2002. The putative tumor suppressor RASSF1A homodimerizes and heterodimerizes with the Ras-GTP binding protein Nore1. Oncogene **21:**1381–1390.
22. **Pfeifer, F. P., J. H. Yoon, L. Liu, S. Tommasi, S. P. Wilczynski, and R. Dammann.** 2002. Methylation of the RASFF1A gene in human cancers. Biol. Chem. **383:**907–914.
23. **Pizzi, S., C. Azzoni, D. Bassi, L. Bottarelli, M. Milione, and C. Bordi.** 2003. Genetic alterations in poorly differentiated endocrine carcinomas of the gastrointestinal tract. Cancer **98:**1273–1282.
24. **Ramirez-Solis, R., P. Liu, and A. Bradley.** 1995. Chromosome engineering in mice. Nature **378:**720–724.
25. **Rong, R., W. Jin, J. Zhang, M. S. Sheikh, and Y. Huang.** 2004. Tumor suppressor RASSF1A is a microtubule-binding protein that stabilizes microtubules and induces G_2/M arrest. Oncogene **23:**8216–8230.
26. **Sakamoto, N., T. Terai, Y. Ajioka, S. Abe, O. Kobayasi, S. Hirai, O. Hino, H. Watanabe, N. Sato, T. Shimoda, and H. Fujii.** 2003. Frequent hypermethylation of RASSF1A in early flat-type colorectal tumors. Oncogene **23:**8900–8907.
27. **Schaft, J., R. Ashery-Padan, F. van der Hoeven, P. Gruss, and A. F. Stewart.** 2001. Efficient FLP recombination in mouse ES cells and oocytes. Genesis **31:**6–10.
28. **Schagdarsurengin, U., L. Wilkens, D. Steinemann, P. Flemming, H. H. Kreipe, G. P. Pfeifer, B. Schlegelberger, and R. Dammann.** 2003. Frequent epigenetic inactivation of the RASSF1A gene in hepatocellular carcinoma. Oncogene **22:**1866–1871.
29. **Sharan, S. K., M. Morimatsu, U. Albrecht, D. S. Lim, E. Regel, C. Dinh, A. Sands, G. Eichele, P. Hasty, and A. Bradley.** 1997. Embryonic lethality and radiation hypersensitivity mediated by Rad51 in mice lacking Brca2. Nature **386:**804–810.
30. **Shima, N., S. A. Hartford, T. Duffy, L. A. Wilson, K. J. Schimenti, and J. C. Schimenti.** 2003. Phenotype-based identification of mouse chromosome instability mutants. Genetics **163:**1031–1040.
31. **Shing, D. C., C. A. Morley-Jacob, I. Roberts, E. Nacheva, and N. Coleman.** 2002. Ewing's tumour: novel recurrent chromosomal abnormalities demonstrated by molecular cytogenetic analysis of seven cell lines and one primary culture. Cytogenet. Genome Res. **97:**20–27.
32. **Shivakumar, L., J. Minna, T. Sakamaki, R. Pestell, and M. A. White.** 2002. The RASSF1A tumor suppressor blocks cell cycle progression and inhibits cyclin D1 accumulation. Mol. Cell. Biol. **22:**4309–4318.
33. **Song, M. S., S. J. Song, N. G. Ayad, J. S. Chang, J. H. Lee, H. K. Hong, H. Lee, N. Choi, J. Kim, H. Kim, J. W. Kim, E. J. Choi, M. W. Kirschner, and D. S. Lim.** 2004. The tumour suppressor RASSF1A regulates mitosis by inhibiting the APC-Cdc20 complex. Nat. Cell Biol. **6:**129–137.
34. **Su, T. T., and J. Stumpff.** 9 March 2004, posting date. Promiscuity rules? The dispensability of cyclin E and Cdk2. Sci. STKE **224:** pe11. [Online.] http://stke.sciencemag.org/cgi/content/full/OC_sigtrans;stke.2242004pe11.
35. **To, K. F., W. K. Leung, T. L. Lee, J. Yu, J. H. Tong, M. W. Chan, E. K. Ng, S. C. Chung, and J. J. Sung.** 2002. Promoter hypermethylation of tumor-related genes in gastric intestinal metaplasia of patients with and without gastric cancer. Int. J. Cancer **102:**623–628.
36. **van der Weyden, L., D. J. Adams, L. W. Harris, D. Tannahill, M. J. Arends, and A. Bradley**. 2005. Null and conditional *Semaphorin* 3B alleles using a flexible *puro*Δ*tk LoxP*/*FRT* vector. Genesis **41:**171–178.
37. **van Engeland, M., G. M. Roemen, M. Brink, M. M. Pachen, M. P. Weijenberg, A. P. de Bruine, J. W. Arends, P. A. van den Brandt, A. F. de Goeij, and J. G. Herman.** 2002. K-ras mutations and RASSF1A promoter methylation in colorectal cancer. Oncogene **21:**3792–3795.
38. **Vos, M. D., C. A. Ellis, A. Bell, M. J. Birrer, and G. J. Clark.** 2000. Ras uses the novel tumor suppressor RASSF1 as an effector to mediate apoptosis. J. Biol. Chem. **275:**35669–35672.
39. **Vos, M. D., A. Martinez, C. Elam, A. Dallol, B. J. Taylor, F. Latif, and G. J. Clark.** 2004. A role for the RASSF1A tumour suppressor in the regulation of tubulin depolymerisation and genomic instability. Cancer Res. **64:**4244–4250.
40. **Wagner, K. J., W. N. Cooper, R. G. Grundy, G. Caldwell, C. Jones, R. B. Wadey, D. Morton, P. N. Schofield, W. Reik, F. Latif, and E. R. Maher.** 2002. Frequent RASSF1A tumour suppressor gene promoter methylation in Wilms' tumour and colorectal cancer. Oncogene **21:**7277–7282.
41. **Wang, J., J. J. Lee, L. Wang, D. D. Liu, C. Lu, Y. H. Fan, W. K. Hong, and L. Mao.** 2004. Value of p16INK4a and RASSF1A promoter hypermethylation in prognosis of patients with resectable non-small cell lung cancer. Clin. Cancer Res. **10:**6119–6125.
42. **Wistuba, I. I., C. Behrens, A. K. Virmani, G. Mele, S. Milchgrub, L. Girard, J. W. Fondon, H. R. Garner, B. McKay, F. Latif, M. I. Lerman, S. Lam, A. F. Gazdar, and J. D. Minna.** 2000. High resolution chromosome 3p allelotyping of human lung cancer and preneoplastic/preinvasive bronchial epithelium reveals multiple, discontinuous sites of 3p allele loss and three regions of frequent breakpoints. Cancer Res. **60:**1949–1960.
43. **Yang, Q., P. Zage, D. Kagan, Y. Tian, R. Seshadri, H. R. Salwen, S. Liu, A. Chlenski, and S. L. Cohn.** 2004. Association of epigenetic inactivation of RASSF1A with poor outcome in human neuroblastoma. Clin. Cancer Res. **10:**8493–8500.
44. **Zhong, S., W. Yeo, M. W. Tang, N. Wong, P. B. Lai, and P. J. Johnson.** 2003. Intensive hypermethylation of the CpG island of Ras association domain family 1A in hepatitis B virus-associated hepatocellular carcinomas. Clin. Cancer Res. **9:**3376–3382.
45. **Zumbrunn, J., K. Kinoshita, A. A. Hyman, and I. S. Näthke.** 2001. Binding of the adenomatous polyposis coli protein to microtubules increases microtubule stability and is regulated by GSK-3β phosphorylation. Curr. Biol. **11:**44–49.